JOURNAL OF COMPUTATIONAL PHYSICS **136,** 168–179 (1997)
ARTICLE NO. CP975765

A Combined Wormlike-Chain and Bead Model for Dynamic Simulations of Long Linear DNA

Hongmei Jian* and Alexander V. Vologodskii†

*Department of Physics and †Department of Chemistry, 4 Washington Place, New York University, New York, New York 10003
E-mail: *jianh@acf2.nyu.edu and †avologod@jethro.cims.nyu.edu

and

Tamar Schlick[1]

Department of Chemistry and Courant Institute of Mathematical Science, New York University and the Howard Hughes Medical Institute, 251 Mercer Street, New York, New York 10012
E-mail: schlick@nyu.edu

Received October 14, 1996; revised May 1, 1997

A carefully parameterized and tested simulation procedure for studying the dynamic properties of long linear DNA, based on a representation that combines features of both wormlike-chain and bead models, is presented. Our goals are to verify the model parameters and protocols with respect to all relevant experimental data and equilibrium simulations, to choose the most efficient algorithms, and to test different approximations that increase the speed of the computations. The energy of the linear model chain includes stretching, bending, and electrostatic components. Beads are associated with each vertex of the chain in order to specify the hydrodynamic properties of the DNA. The value of the stretching rigidity constant is chosen to achieve a compromise between the efficiency of the dynamic simulations (since the timestep depends on the stretching constant) and realistic modeling of the DNA (i.e., small deviations of the input contour length); the bead hydrodynamic radius is set to yield agreement with known values of the translational diffusion coefficient. By comparing results from both a first- and a second-order Brownian dynamics algorithm, we find that the two schemes give reasonable accuracy for integration timesteps in the range 200–500 ps. However, the greater accuracy of the second-order algorithm permits timesteps of 600 ps to be used for better accuracy than the 300 ps used in the first-order method. We develop a more efficient second-order algorithm for our model by eliminating the auxiliary calculations of the translational diffusion tensor at each timestep. This treatment does not sacrifice accuracy and reduces the required CPU time by about 50%. We also show that an appropriate monitoring of the chain topology ensures essentially no intrachain crossing. The model details are assessed by comparing simulation-generated equilibrium and dynamic properties with results of Monte Carlo simulations for short linear DNA (300, 600 base pairs) and with experimental results. Very good agreement is obtained with Monte Carlo results for distributions of the end-to-end distance, bond lengths, bond angles between adjacent links, and translational diffusion measurements. Additionally, comparison of translational diffusion coefficients with experimentally-measured values for DNA chains (of 367, 762, 1010, 2311 base pairs) shows excellent agreement as well. This lends confidence to the predictive ability of our model and sets the groundwork for further work on circular DNA. We conclude with results of such a predictive measurement, the autocorrelation time, for the end-to-end distance and the bending angle as a function of DNA length. Rotational diffusion measurements for different DNA lengths (300 to 2311 base pairs) are also presented. © 1997 Academic Press

1. INTRODUCTION

The large-scale dynamic motions of double helical DNA are important for many biological processes, from protein/DNA interactions to higher-order DNA folding and recombination. Several approaches have been developed during the past decade to model DNA dynamics on the basis of low-resolution models [3, 4, 6, 7, 24, 29, 31, 32, 35]. Such approaches allow simulation of slow motions in long DNA molecules that are not possible to capture with standard all-atom simulations, unfortunately limited to several dozen residues. However, modeling slow motions in large DNA molecules remains a challenge. In particular, it is difficult to simulate slow processes in double-stranded supercoiled DNA where torsional rotation of the chain segments is important. This is a broad objective of the simulation protocol developed here. In this paper, we focus on linear DNA. In a second work [20] we continue to treat closed circular DNA, where additional terms are required, and to study biological questions. In particular, our goals here are to verify the model parameters and protocols with respect to all relevant experimental data and equilibrium simulations, to choose the most efficient algorithms, and

[1] To whom correspondence should be addressed.

0021-9991/97 $25.00
Copyright © 1997 by Academic Press
All rights of reproduction in any form reserved.

to test different approximations to increase the speed of the computations.

Our model is based on the classical discrete wormlike chain and is close to the approach introduced by Allison and McCammon [4]. It combines the wormlike chain features with those of a bead model, which has been used extensively for polymer hydrodynamics. The working model accounts for two essential features of the double helix: the bending potential and the electrostatic interaction between chain segments. Electrostatic interactions are not standard components of Brownian simulations [2, 6, 7]. Electrostatic contributions are significant for the conformational properties of long DNA molecules, especially in compact topologically constrained circular DNA [21, 28, 30, 33, 37]. An explicit electrostatic potential also offers a computational advantage over a simple excluded-volume term since its smoothness allows the use of larger integration timesteps without force-discontinuity artifacts. An electrostatic potential has recently been added [8] to the DNA model of Chirico and Langowski [7], but details are lacking in that work, as well as a description of how different salt concentrations are modeled. Our model also contains a stretching potential to facilitate dynamic simulations. The effect of the stretching rigidity constant on obtained dynamic properties of the model is also closely examined in this work.

Details of our computational procedure are presented, along with discussions of parameter choices. Model details are assessed through comparisons of results to equilibrium simulations for the same model, as well as to available experimental data (translational diffusion coefficients). Excellent agreement is obtained for all equilibrium and dynamic properties examined (e.g., end-to-end distance, bending distributions, persistence length, and translational diffusion coefficients).

For generation of molecular trajectories, we rely on the theoretical framework of the generalized Langevin equation used previously in the simplest form by Schlick *et al.* [31, 26]. Here, we use the Brownian dynamics (diffusive) regime to study the long-time motion of large-scale DNA systems.

Following the description of our model in Section 2 and a description of the simulation algorithms (integration and Monte Carlo) in Section 3, we discuss in Section 4 the parameterizations of the stretching-rigidity constants and hydrodynamic bead radius, as well as the selection of the dynamic algorithm and associated timestep. In Section 5, simulation results are presented for the distribution function of end-to-end distance, translational diffusion constant, autocorrelation functions, and rotational diffusion constant.

We emphasize that our focus in this work is a careful and detailed development of a macroscopic computational model for dynamic simulations, addressing all issues of potential functions, chain representation, and propagation algorithms. Such issues must be satisfactorily completed to ensure that there are no artifacts in later results. The excellent agreement obtained with respect to available Monte Carlo, theoretical, and experimental data establishes a reliable and efficient protocol for dynamic simulations of long DNA. Extensions to circular DNA and to site-juxtaposition studies have already been described in the Ph.D. thesis of Jian [19], and will be published separately [20].

2. THE MODEL

Our energy model for linear DNA includes stretching (E^s), bending (E^b), and electrostatic (E^e) potentials. A DNA molecule composed of m Kuhn statistical lengths (each Kuhn length is 300 base pairs) is modeled by N beads of radius a linked by $N-1$ virtual bonds. The equilibrium "bond length" (link), l_0, between beads is chosen according to the salt concentration of the solution (see below); it is thus related to the Debye length.

The bond stretching energy, a computational device (restraint), is expressed as

$$E^s = \frac{h}{2} \sum_{i=1}^{N-1} (l_i - l_0)^2. \tag{2.1}$$

The choice of the stretching force constant, h, must balance computational requirements with realized deviations of the bond.

The elastic bending potential of the chain E^b is computed as

$$E^b = \frac{g}{2} \sum_{i=1}^{N-2} \theta_i^2, \tag{2.2}$$

where θ_i is the angular displacement of bond i relative to bond $i+1$, and g is the bending rigidity constant. This parameter is related to the DNA persistence length p [11, 15] and is determined by the procedure described by Frank-Kamenetskii *et al.* [12], summarized for completeness in Appendix A.

The electrostatic intersegment interaction of our DNA chain is described by the Debye–Hückel (DH) potential. In practice, a point charge, νl_0, is attributed to each vertex and E^e is defined as

$$E^e = \sum_{j>i+1} \frac{\nu^2 l_0^2}{D} \frac{\exp(-\kappa r_{ij})}{r_{ij}}, \tag{2.3}$$

where ν is the effective linear charge density, D is the dielectric constant, r_{ij} is the distance between vertices i and j, and κ is the inverse of the Debye length. The value

ν corresponds to the best approximation for the Poisson–Boltzmann solution for DNA, modeled as a charged cylinder by the DH potential [34]; see references [30] and [38], for example, for specific values. The Debye length is taken as

$$r_D = 1/\kappa = \sqrt{\frac{Dk_{\mathrm{B}}T}{8\pi e^2 c_{\mathrm{s}}}}, \tag{2.4}$$

where c_{s} is the molar salt concentration of monovalent ions. In this work, we set $c_{\mathrm{s}} = 0.01\ M$, $D = 80$ (aqueous medium), and ν is set according to Ref. [38]: $\nu = 0.243e/\mathrm{A}$, where e is the charge of an electron. At room temperature ($T = 298$ K), the corresponding value of r_D is 3.07 nm. Additional torsional and torsional/bending terms are necessary for closed circular DNA (see [17] for example); they are not used in the current work.

To associate hydrodynamic properties for our DNA model, we place virtual beads of radius a and mass m at each vertex of our model chain. The generalized Langevin equation of translational motion can be expressed as

$$m\dot{\mathbf{v}}_i = -\sum_{j=1}^{N} \boldsymbol{\xi}_{ij} \cdot \mathbf{v}_i + \boldsymbol{F}_i + \sum_{j=1}^{N} \boldsymbol{\alpha}_{ij} \cdot \mathbf{f}_j, \qquad 1 \le i \le N, \tag{2.5}$$

where $\mathbf{v}_i$ is the velocity of the ith bead, $\mathbf{F}_i$ is the sum of interparticle forces acting on bead i, and $\sum_j \boldsymbol{\alpha}_{ij} \cdot \mathbf{f}_j$ represents the randomly fluctuating force. The translational friction tensor, $\boldsymbol{\xi}_{ij}$, is connected to stochastic forces via

$$\boldsymbol{\xi}_{ij} = \frac{1}{k_B T} \sum_l \boldsymbol{\alpha}_{il} \cdot \boldsymbol{\alpha}_{lj}^{\mathrm{T}}. \tag{2.6}$$

The friction tensor is also related to the translational diffusion tensor

$$\overline{\mathbf{D}}_{ij} = \frac{k_{\mathrm{B}}T}{\boldsymbol{\xi}_{ij}}, \tag{2.7}$$

where $\overline{\mathbf{D}}_{ij}$ can be defined by the Rotne–Prager [27] hydrodynamic interaction tensor. For clarity, we use $\mathbf{D}$ to denote the $3N \times 3N$ translational diffusion matrix. This symmetric configuration-dependent matrix can be written as a collection of 3×3 subblock matrices $\overline{\mathbf{D}}_{ij}$ for each pair of particles (i and j):

$$\mathbf{D} = \begin{pmatrix} \overline{\mathbf{D}}_{11} & \overline{\mathbf{D}}_{12} & \cdot & \cdot & \overline{\mathbf{D}}_{1N} \\ \overline{\mathbf{D}}_{21} & \overline{\mathbf{D}}_{22} & \cdot & \cdot & \overline{\mathbf{D}}_{2N} \\ \cdot & \cdot & \cdot & \cdot & \cdot \\ \overline{\mathbf{D}}_{N1} & \overline{\mathbf{D}}_{N2} & \cdot & \cdot & \overline{\mathbf{D}}_{NN} \end{pmatrix}. \tag{2.8}$$

For $i = j$, each 3×3 subblock is given by

$$\overline{\mathbf{D}}_{ij} = \frac{k_{\mathrm{B}}T}{6\pi\eta a} \mathbf{I}_{3\times 3}. \tag{2.9}$$

For $i \neq j$, in the case of nonoverlapping beads ($r_{ij} > 2a$), we have

$$\overline{\mathbf{D}}_{ij} = \frac{k_{\mathrm{B}}T}{8\pi\eta r_{ij}} \left[\left(\mathbf{I}_{3\times 3} + \frac{\mathbf{r}_{ij}\mathbf{r}_{ij}}{r_{ij}^2} \right) + \frac{2a^2}{r_{ij}^2} \left(\frac{1}{3} \mathbf{I}_{3\times 3} - \frac{\mathbf{r}_{ij}\mathbf{r}_{ij}}{r_{ij}^2} \right) \right], \tag{2.10}$$

and for overlapping beads

$$\overline{\mathbf{D}}_{ij} = \frac{k_{\mathrm{B}}T}{6\pi\eta a} \left[\left(1 - \frac{9}{32} \frac{r_{ij}}{a} \right) \mathbf{I}_{3\times 3} + \frac{3}{32} \frac{\mathbf{r}_{ij}\mathbf{r}_{ij}}{a r_{ij}} \right]. \tag{2.11}$$

In the expression above, $\mathbf{r}_{ij}$ is the three-dimensional distance vector between beads i and j, and η is the viscosity of the solvent. In the simulations reported here we use the nonoverlapping beads case, except for the calibration work described in connection with the hydrodynamic radius.

3. SIMULATION ALGORITHMS AND PERFORMANCE

3.1. *Monte Carlo*

We first describe the Metropolis Monte Carlo (MC) procedure to simulate equilibrium conformational distributions of linear DNA chains. These results are later compared to those generated by our dynamic simulations.

Two types of perturbation moves are used (see Fig. 1). Move (a) is local: one vertex (bead) is randomly selected and a random displacement $\mathbf{r}$ is applied. The random vector is uniformly distributed in the space, and its length is in the range of $[0, \delta_1^0]$ (where the upper bound δ_1^0 is determined by the acceptance ratio).

Move (b) is global. After a random vertex is selected, a rotation of the shorter part of the chain with respect to a random axis which passes through the selected vertex is applied. The orientation of the axis is uniformly distributed in space, and the rotation angle applied for the move is uniformly distributed in the range of $[0, \delta_2^0]$, where δ_2^0 is the upper bound determined by the acceptance ratio.

The probability of accepting a trial conformation is obtained by applying the standard rules of Metropolis *et al.* [23]. Namely, if the total potential energy of the trial conformation, E_{new}, is lower than that of the previous conformation, E_{old}, the trial conformation was accepted. If $E_{\mathrm{new}} > E_{\mathrm{old}}$, the probability of acceptance of the trial conformation is made equal to $p_{\mathrm{acc}} = \exp[(E_{\mathrm{old}} - E_{\mathrm{new}}]/k_{\mathrm{B}}T)$. In practice this is accomplished by comparing a random number x (uniformly distributed in [0, 1]) with p_{acc}; if $x >$

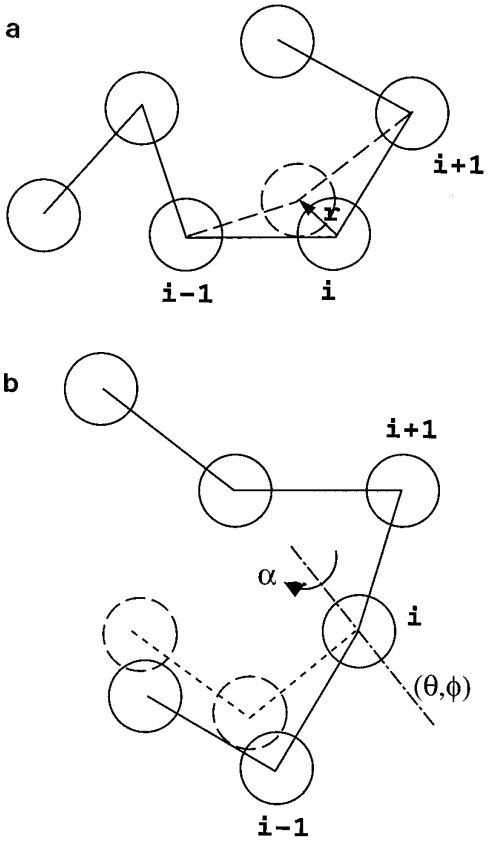

FIG. 1. Two types of Monte Carlo moves: (a) local, random bead displacement and (b) global, random axis rotation.

p_{acc}, the new conformation is accepted, but otherwise the old conformation is recounted. The combined protocol (for using both moves) is calibrated (i.e., setting δ_1^0 and δ_2^0) so that the acceptance ratio of either of the moves is around 50%, and the probability of selecting the two types of moves is equal.

3.2. *Dynamics*

The generalized Langevin equation (Eq. (2.5)) provides the reference for the generation of molecular trajectories. In the Brownian limit of small inertial contributions and sufficiently large timesteps (exceeding momentum relaxation time of the particles), the propagation can be simplified [10]. We tested two Brownian dynamics (BD) algorithms with respect to accuracy and efficiency. The common BD algorithm by Ermak and McCammon [10] (first-order) generates the new position vector for the beads, $\mathbf{x}^{n+1}$, from the current positions, $\mathbf{x}^n$, according to the formula

$$\mathbf{x}^{n+1} = \mathbf{x}^n + \frac{\Delta t}{k_{\text{B}}T}\mathbf{D}^n \cdot \mathbf{F}^n + \mathbf{R}^n, \tag{3.1}$$

where $\mathbf{D}^n$ is the translational diffusion matrix and $\mathbf{F}^n$ is the collective vector of interparticle forces, as defined above. The random force, $\mathbf{R}^n$, is generated at each step from a Gaussian distribution of mean zero and variance

$$\langle \mathbf{R}^n \mathbf{R}^{n'} \rangle = 2\mathbf{D}^n \, \Delta t \delta_{nn'}, \tag{3.2}$$

where $\delta_{nn'}$ is the Kronecker delta symbol. We follow the procedure described in Ref. [10] to generate the components of $\mathbf{R}$. This involves setting $\mathbf{R}$ to a linear combination of $3N$ normal random deviates. The computational complexity of this task is of order $(3N)^3$.

The second-order algorithm was developed and applied by Iniesta and Garcia de la Torre for Trumbell dynamics [18] and also used by Chirico and Langowski for a DNA model [6, 7]. This scheme generates $\mathbf{x}^{n+1}$ in two steps. First, Eq. (3.1) is used to generate an auxiliary position vector, $\tilde{\mathbf{x}}^{n+1}$. Second, the following formula is used to generate the new position vector

$$\mathbf{x}^{n+1} = \mathbf{x}^n + \frac{1}{2}\frac{\Delta t}{k_{\text{B}}T}\left(\mathbf{D}^n \cdot \mathbf{F}^n + \tilde{\mathbf{D}}^{n+1} \cdot \tilde{\mathbf{F}}^{n+1}\right) + \tilde{\mathbf{R}}^{n+1}.$$

$$\langle \tilde{\mathbf{R}}^{n+1} \tilde{\mathbf{R}}^{n+1} \rangle = (\mathbf{D}^n + \tilde{\mathbf{D}}^{n+1}) \, \Delta t, \qquad \langle \tilde{\mathbf{R}}^{n+1} \rangle = 0, \tag{3.3}$$

where $\tilde{\mathbf{D}}^{n+1}$ and $\tilde{\mathbf{F}}^{n+1}$ are calculated using the values of $\tilde{\mathbf{x}}^{n+1}$. This algorithm requires approximately twice the CPU time as the first-order scheme.

Both algorithms are based on the assumption that the motions of interest occur on a time scale much larger than the momentum relaxation time, i.e., $\Delta t \gg mD_{ii}/k_{\text{B}}T = m/(6\pi\eta a)$, where D_{ii} is the ith diagonal entry of $\mathbf{D}$, and m is the mass of the bead. In our case, when all bond lengths are $l_0 = 5$ nm and the hydrodynamic radius of a bead is $a = 1.78$ nm, this lower bound for the timestep is 0.5 ps. Timesteps larger than 10 ps were tested in this work.

To improve the computational performance, we suggest modifying the second-order algorithm above by eliminating the calculation of $\tilde{\mathbf{D}}$ and $\tilde{\mathbf{R}}$ in the second phase. That is, the previous $\mathbf{D}$ and $\mathbf{R}$ are reused instead of formulating new values from Eq. (3.3). We found that this modification yields the same accuracy while reducing the CPU time by about 50%.

3.3. *Computational Performance*

Simulations were performed in serial mode on a Silicon Graphics Power Challenge computer with four 75 MHZ IP21 processors. For a model chain of 41 beads (600 base pairs), a simulation of one million MC iterations requires 11 min. In comparison, one million iterations of the Ermak and McCammon algorithm with a timestep of 300 ps (covering 0.3 ms) require 280 min. Our modified second-order scheme with a timestep of 600 ps requires 162 min

to cover the same total simulation time. Some simulations were also performed on a Silicon Graphics Power Challenge with eight 90 MHZ IP21 processors at Cornell Theory Center, which is faster than the 75 MHZ computer by roughly 15%.

4. MODEL PARAMETERS

4.1. *Bond Length and Rigidity Constant*

For reference, we introduce the parameter k to denote the number of beads per Kuhn length. Thus, $k = N/m = 2p/l_0$, where p is the persistence length. There are two requirements in selecting the value of k. First, k must be sufficiently large so that the electrostatic interaction of the discrete charges approximates well the interaction of continuously charged segments. Vologodskii and Cozzarelli [38] found that the condition of $l_0 < 2r_D$ provides a reasonable approximation. Since the static persistence length of DNA is 50 nm, this condition gives a lower limit of $k = 17$ under salt concentration of 0.01 M. Second, the chosen value of k must prevent chain crossings.

As a test, we checked the conservation of topology of a circular chain by calculating the Alexander polynomial at the point -1 [13]. We started the Brownian dynamics simulation from a chain conformation corresponding to a trefoil knot. For the short chain (600 base pairs) used, the equilibrium fraction of knotted conformations is known to be extremely low [13], so any strand passage during the course of dynamic simulations should unknot the DNA. We found that the chain topology is unchanged for more than 10^6 steps if k is larger than 20. However, when $k = 10$, for example, unknotting takes place in less than 1000 steps. Thus, $k = 20$ is appropriate to simulate the DNA dynamics for the monovalent salt concentration of 0.01 M. The corresponding bond length, l_0, is 5 nm, and the corresponding bending rigidity constant is $g = 9.820\ k_B T$ [12] (see Appendix A for a brief description). This force constant can be related to the conventional A values used in other works, in the curvature-squared integral ($A/2 \int \kappa^2(s)\ ds$), according to $A = 2.02 \times 10^{-19}$ erg · cm if $p = 50$ nm.

The value of the stretching rigidity constant, h, is closely related to the choice of timestep in the dynamic simulations. Indeed, during one timestep the force acting on each bead should not change significantly. However, too small a value for h would permit large deviations from equilibrium lengths. A good compromise is obtained by choosing h so that the resulting deviations from l_0 satisfy

$$\frac{\sigma}{l_0} = \frac{\sqrt{\langle l^2\rangle - \langle l\rangle^2}}{l_0} = 0.1. \tag{4.1}$$

The expected value for σ can be obtained from the following general formula for the ith moment of bond length, l, when only the stretching potential is considered:

$$\begin{aligned}\langle l^i\rangle &= \frac{\int l^i \exp(-E^s/k_B T)\, dV}{\int \exp(-E^s/k_B T)\, dV} \\ &= \frac{\int_0^\infty \exp(-h(l-l_0)^2/2k_B T) 4\pi l^{i+2}\, dl}{\int_0^\infty \exp(-h(l-l_0)^2/2k_B T) 4\pi l^2\, dl}.\end{aligned} \tag{4.2}$$

The above two equations can be solved numerically for various input values of h. Then by experimentation, the condition in Eq. (4.1) gives approximately $h = 100\ k_B T/l_0^2$ and corresponds to the value chosen by Allison [2]. This value of h yields in turn values for $\langle l\rangle/l_0$ of 1.020.

We checked that for this value of h and larger the relaxation times of the end-to-end distance were the same within the accuracy of our calculations, about 10%. Furthermore, we also computed mean square end-to-end distance, $\langle L^2\rangle$, from MC simulations. For a system of 3000-bp DNA, the simulation result of $\langle L^2\rangle$ deviated only 5.0% from that of a continuous wormlike chain. In dynamic simulations, the choice $h = 100\ k_B T/l_0^2$ allows us to use a timestep as large as 500 ps (see below).

4.2. *Bead Radius*

The radius of each bead in our model, a, was chosen to yield the same value of frictional coefficient as that of the well-studied model of touching beads. The model of touching beads predicts correct hydrodynamic properties of DNA when $a = 1.59$ nm [16]. Using the Monte Carlo procedure we generated conformational ensembles of 10^5 states for touching ($k = 31.45$) and nontouching beads ($k = 20$), the latter corresponding to our model. Then we used each set to calculate the corresponding translational frictional coefficient, f_0. This coefficient was calculated by the direct solution of the Burgers–Oseen problem as proposed by Zimm [39]. This procedure involves obtaining the ensemble average of the sedimenting velocity, $\langle u_z\rangle$, and then calculating f_0 via the relation

$$f_0 = F/\langle u_z\rangle, \tag{4.3}$$

where F is the sedimenting force. Thus, the translation diffusion constant can be estimated from an equilibrium simulation by assuming rigid-body motion. For completeness, the procedure is summarized in Appendix B.

We found the value $a = 1.78$ nm to give the same value of frictional coefficient as the touching bead model. This value was also independent of chain length. For reference, the principle of equivalent chain volume suggested by

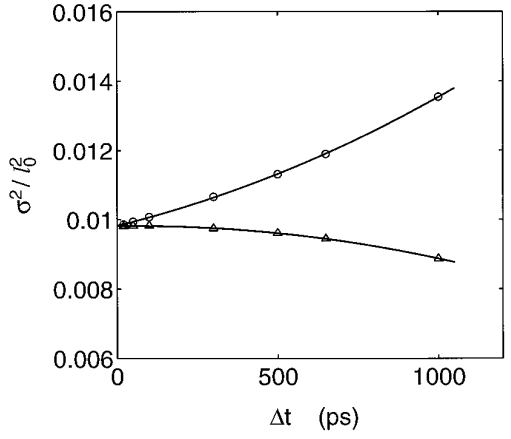

FIG. 2. The variance of the bond length, σ^2, given as σ^2/l_0, where l_0 is the equilibrium bond value, as a function of timestep (Δt) for two BD algorithms, first-order [10] (open circles) and second-order [18, 6] (open triangles). In these simulations, the DNA chain has 600 bp (two Kuhn statistical segments, each segment represented by $k = 20$ links) and the stretching constant $h = 100\ k_B T/l_0^2$ is used (Eq. (2.1)). Statistical errors for both schemes are less than 0.2%.

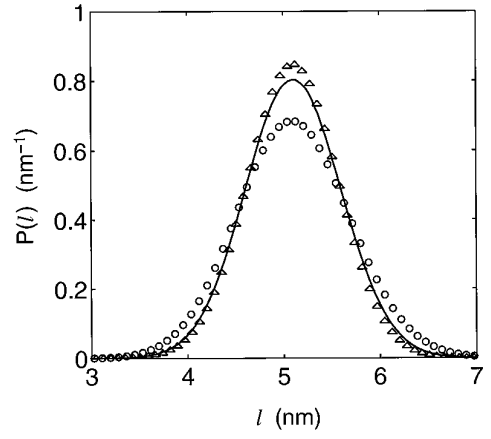

FIG. 3. Distribution functions of a representative bond length (normalized), as obtained from the two BD algorithms for $\Delta t = 1000$ ps: first-order (open circles) and second-order (open triangles) versus MC (solid line). The chain is 600 bp long. The trajectory lengths for BD are both 1.0 ms and, for MC, 4 million conformations were generated.

de la Torre and Bloomfield [14] for choosing a gives the close value of 1.85 nm.

4.3. *Dynamic Algorithms and Timestep*

We tested two different BD algorithms as discussed in Section 3.2 with various timesteps, Δt. Several local and global properties of the chain, both equilibrium and dynamic, were assessed. These include distribution functions of bond length, bond angle, and end-to-end distance; the translational diffusion coefficient; autocorrelation functions for the end-to-end distance and bending angle; and the rotational diffusion coefficient. We found the variance of the bond length, σ^2, to be most sensitive to Δt. This is expected since the stretching potential has the highest motion frequency in our model.

Figure 2 shows the dependence of σ^2 (normalized) on Δt for the first and second-order BD algorithms, and Fig. 3 shows the distribution functions of a representative bond length for the two BD algorithms with $\Delta t = 1000$ ps versus the MC result. As Δt increases, we see that σ^2 increases in magnitude but, as expected, the second-order algorithm is more accurate (smaller deviations). Although the CPU time for one iteration of the second-order method is double that of the first-order algorithm (compare Eq. (3.3) with Eq. (3.1)), the former tolerates a Δt at least two times larger for the same accuracy. Note, for example, from Fig. 2 that the error from the first-order scheme at $\Delta t = 300$ ps is about the same as the error realized by the second-order BD method for $\Delta t = 1000$ ps. For further efficiency, our modified version of the second-order algorithm was used. This modification does not change the results significantly (data not shown), but saves 50% of the CPU time. This can be seen from Table I, which shows the corresponding CPU time for the three algorithms.

For most calculations in this work, we used our modified second-order algorithm with a timestep of 600 ps. Less than 2% difference was found for the average value of the

TABLE I

CPU Time for Different BD Algorithms for Covering 60 Microseconds

Number Beads/Base Pairs	First-Order (min)	Second-Order (min)	Modified Second-Order (min)	Speedup Ratio
41/600	56.0	54.9	32.8	1.67
68/1010	173.2	171.4	99.7	1.72
101/1500	437.6	435.3	249.4	1.75

Note. A timestep of 300 ps was used for the first-order scheme, with 600 ps for the second-order methods. The simulations were run on an SGI Power Challenge computer with eight 90 MHZ IP21 processors in serial mode.

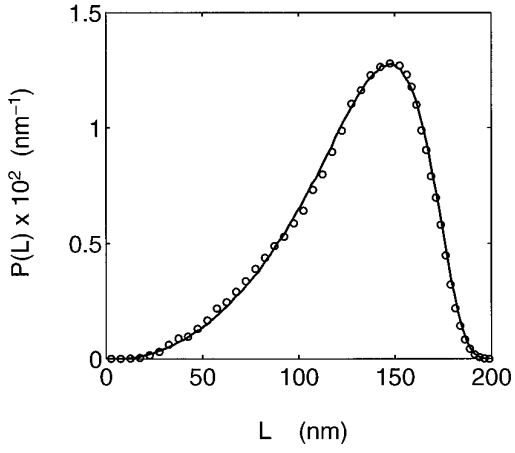

FIG. 4. Comparisons of normalized distribution functions of the end-to-end distance obtained by MC (solid line) over 4 million steps and by BD (open circles) covering 6 ms. A model chain with 41 beads is used (600 bp) at the monovalent salt concentration of 0.01 *M*.

TABLE II

Comparison of the Translational Diffusion Coefficients for Different Lengths of DNA

DNA Length (bp)	D_t ($\times 10^{-8}$ cm^2/s)	D^{MC} ($\times 10^{-8}$ cm^2/s)	D^{Exp} ($\times 10^{-8}$ cm^2/s)
300	16.94 ± 0.11	16.47 ± 0.02	
367	14.79 ± 0.12	15.00 ± 0.02	15.8 ± 0.47
762	8.78 ± 0.15	8.74 ± 0.01	9.05 ± 0.11
1010	7.18 ± 0.13	7.17 ± 0.01	7.15 ± 0.19
2311	4.11 ± 0.12	3.98 ± 0.01	4.56 ± 0.13

Note. D^{Exp} denotes the experimental values for Ref. [25], while D_t and D^{MC} are the simulation value for BD and MC, respectively, as calculated in this work. For each chain length, five different BD trajectories of length of 0.6 ms were used, each with a different initial conformation. Each D^{MC} was obtained from three different MC ensembles (each ensemble a selection of 10^5 conformations out of the total 10^6).

end-to-end distance when smaller values of Δt were used. Statistically significant differences in corresponding autocorrelation functions of the end-to-end distance and rotational diffusion coefficient were not observed with this protocol.

5. SOME SIMULATION RESULTS

5.1. *End-to-End Distance Distribution*

Using the model described above we tested the efficiency of our BD protocol to reproduce the equilibrium end-to-end distance distribution as obtained by MC. Figure 4 shows excellent agreement and demonstrates that it is possible to get statistically reliable results by BD simulations for the model chain in this range of length (600 bp), especially with the speedup of the modified second-order algorithm. MC is computationally more competitive (e.g., factor of 200 here), but inadequate for studying dynamic properties.

5.2. *Translational Diffusion Constant*

In dynamic simulations, the translational diffusion constant, D_t, can be estimated via a long trajectory simulation by relating the mean square fluctuations of the system to D_t according to the Einstein–Stokes equation

$$6tD_t(t) = \langle |\mathbf{x}_{cm}(t) - \mathbf{x}_{cm}(0)|^2 \rangle, \qquad (5.1)$$

where $\mathbf{x}_{cm}(t)$ is the center-of-mass position vector of the DNA chain at time t, and the brackets $\langle \cdot \rangle$ indicate ensemble averaging. Figure 5 shows that there is a certain length of time that provides the best accuracy, around $1000\Delta t$. Statistical errors were also computed from five different trajectories differing in the initial conformation and random seed. The results are shown in Table II together with the corresponding values from MC simulation, D^{MC}, and displayed in Fig. 6 along with the experimental results of references [22] and [25]. The D^{MC} values were obtained by using Einstein's relation of $k_B T/f_0$, where f_0 is the frictional coefficient (see Section 4.2). Although there is a very good agreement between results obtained by two different approaches, differences (1–3%) exceed statistical error (1%) for short chains (300 and 367 bp). It is possible that the rigid-body approximation in the calculations of D^{MC} is responsible for the difference.

From the comparison of our D_t values with the experimental results (D^{Exp}) of Ref. [25] (Table II) and to the

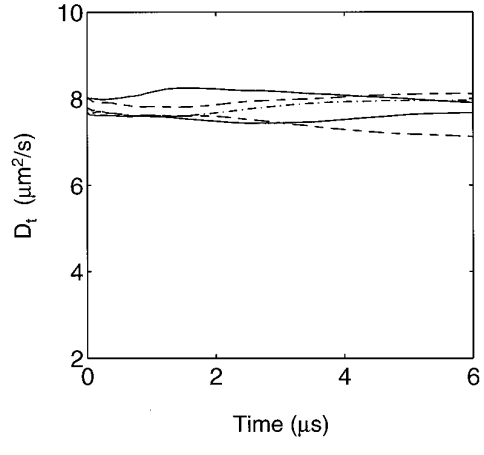

FIG. 5. Convergence of the translational diffusion coefficient, D_t, from BD simulations (Eq. (5.1)) covering 0.6 ms for a model chain of 68 beads (1010 bp). Each trajectory differs by the starting conformation.

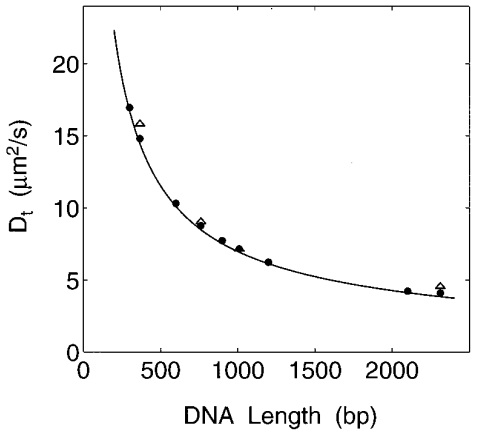

FIG. 6. Comparison of the translational diffusion coefficient, D_t, for different lengths of DNA. The filled circles represent the BD simulation results with $\Delta t = 600$ ps, as obtained from five different trajectories of length 0.6 ms for each chain length. The open circles denote the experimental results of [22], with the solid line representing the best cubic fit described in [22]. The open triangles are the experimental results of [25] shown in Table II.

best fit of experimental results from [22] (Fig. 6), we also note a very good agreement for all the chain lengths used (corresponding to the experimental systems). This lends confidence in the predictive capability of our model.

5.3. *Rotational Diffusion Constant*

The rotational diffusion constant, D_r, can be estimated via the following relation [2] involving the second-order Legendre polynomial, P_2,

$$-\ln\langle P_2(\mathbf{u}(t)\cdot\mathbf{u}(0))\rangle = 6D_r t, \tag{5.2}$$

where $\mathbf{u}(t)$ is the unit vector of the end-to-end distance at time t. In practice, this formula can be used to compute D_r by finding the slope of the slowest component of the curve of $-\ln\langle P_2(\mathbf{u}(t)\cdot\mathbf{u}(0)\rangle$ versus t. The decay of P_2 is well described by a single exponential only for short DNA, and as the DNA length increases, this decay is generally described by several exponential terms. Figure 7 shows examples of semilog plots of the decay of P_2 versus t for a short DNA (300 bp, Fig. 7a) and for a longer DNA system (1500 bp, Fig. 7b). We see that a single-exponent approximation is accurate for the short chain only.

Figure 8 shows the results of the corresponding rotational relaxation time, $\tau = 1/(6D_r)$, for different DNA lengths. Because of the multiexponential nature of decay for longer chains, the τ values shown only correspond to the slowest motion of the polymer. Note that the error of D_r in Fig. 8 increases with DNA length. This might be due to the complexity of the relaxation times. Hagerman and Zimm [16] showed that for short chains ($\mathscr{L}/p < 5$), where $\mathscr{L}$ is the contour length and p is the persistence length, the coupling between components produces the largest relaxation time; this slowest component corresponds to the rotation about the longitudinal axis in the rigid-rod limit. Their results for $\mathscr{L}/p < 5$ (750 bp) are also shown in Fig. 8 (dashed line in the inset). For the shortest DNA used in the simulations, our data are in very good agreement with that of Hagerman and Zimm. This agreement also shows that the rigid-body approximation of [16] works well for D_r.

5.4. *Autocorrelation Functions*

For a given time-dependent physical property $A(t)$, the normalized autocorrelation function is defined as [1]

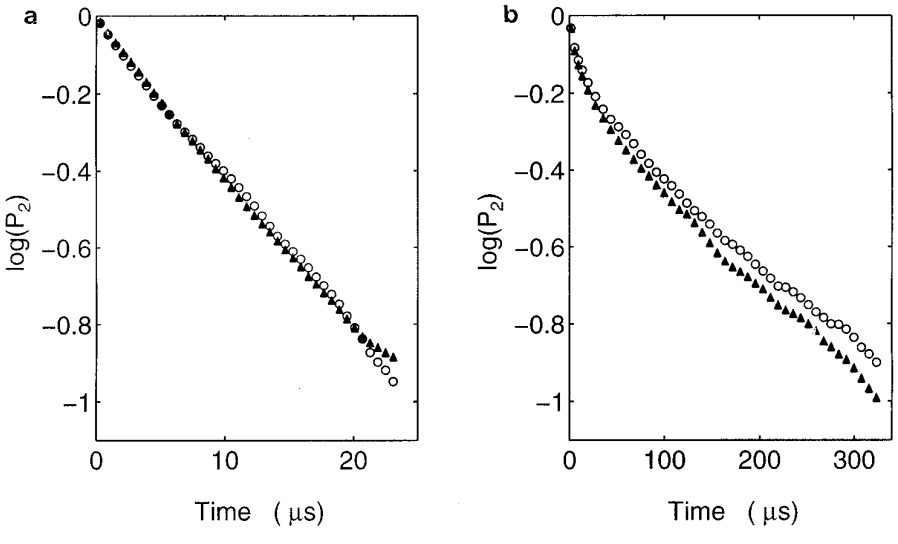

FIG. 7. Evolution of the logarithm of the second-order Legendre polynomial for two different DNA lengths, (a) 300 bp and (b) 1500 bp. For each DNA length, results from two different trajectories are presented (open circles and filled triangles). For a 300-bp linear DNA, the decay of the Legendre polynomial (see Eq. 5.2) is a single exponential (left), but for longer DNA the decay is multiexponential in form (right).

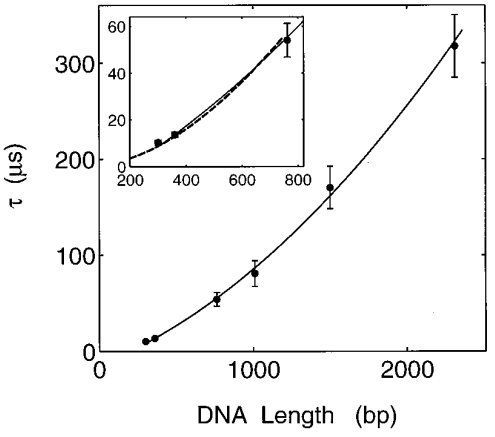

FIG. 8. Rotational relaxation time, τ_r, for different chain lengths (300, 360, 762, 1010, 1500, 2311) as obtained by BD. The filled circles are the BD simulation results, and the solid line is its best cubic fit. Five different trajectories (each of length of 0.6 ms) were performed, each with a different starting conformation. The dashed line in the insert corresponds to results of Ref. [16] (obtained as $\tau_B R_c$ (exact)).

$$c_{AA}(t) = \frac{\langle A(t) \cdot A(0)\rangle - \langle A\rangle^2}{\sigma_A^2}, \tag{5.3}$$

where σ_A^2 is the variance of A. We computed the autocorrelation functions for L and θ, the end-to-end distance and the bending angle, respectively.

Figure 9 shows typical autocorrelation functions for L and θ_i ($i = 1$ and $i = N/2$) as obtained by BD for a 600-bp DNA system. The autocorrelation function of L can be fitted well to an exponential form of $\exp(-t/\tau_L)$ (Fig. 9a). The dependence of τ_L (correlation time of L) on chain length $\mathscr{L}$ is plotted in Fig. 10. This dependence can be approximated by $\tau_L \sim \mathscr{L}^\alpha$, where $\alpha \approx 2$ for small $\mathscr{L}$, with α decreasing for longer DNA. This finding is in qualitative agreement with theoretical results [9], but further quantitative comparisons are unwarranted due to the approximate nature of the τ_L calculations.

The autocorrelation functions for θ_i cannot be fitted to a single exponential (Fig. 9b), but a dependence on the bead index, i, can be seen ($C_{\theta\theta}$ is shown for $i = 1$ and $i = N/2$ where N is the total number of beads). Clearly, the behavior of the end beads of the DNA is expected to be different than that of the central beads. These differences are not very sensitive to $\mathscr{L}$.

6. SUMMARY

We have described the development of a macroscopic computational procedure for simulating both equilibrium (from thermal ensembles) and dynamic properties of long linear DNA. Our model combines features of the standard wormlike chain model—used extensively for simulating equilibrium properties of linear and supercoiled DNA by Monte Carlo—with a bead framework, used historically for Brownian simulations of polymers with hydrodynamics. We have added stretching and electrostatic potentials to make the model applicable to long DNA.

To test the simulation protocol and to select appropriate parameters and algorithms, we explored in detail the choices of the virtual bond length l_0 (salt dependent), the stretching constant (h), and the bead radius (a). We also compared several algorithms for Brownian dynamics and assessed the accuracy obtained for different timesteps. Results were presented for distributions of bond length and

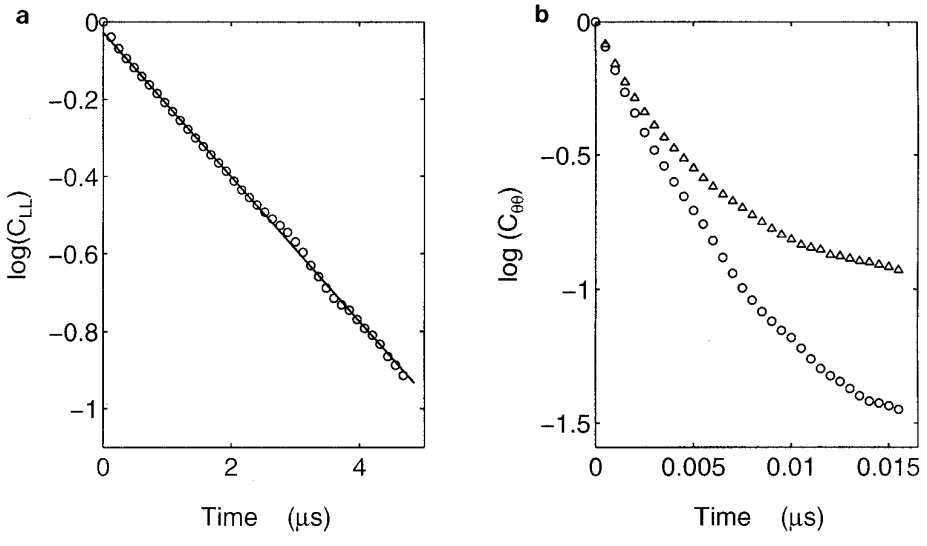

FIG. 9. Autocorrelation functions of (a) the end-to-end distance and (b) the bending angle for a 300-bp DNA. The solid line in part (a) represents the best fit to the form of $\exp(-t/\tau_L)$ with $\tau_L = 2.33$ μs. In part (b), $C_{\theta\theta}$ is shown for two bead indices, $i = 1$ (open circles), and $i = N/2$ (open triangles).

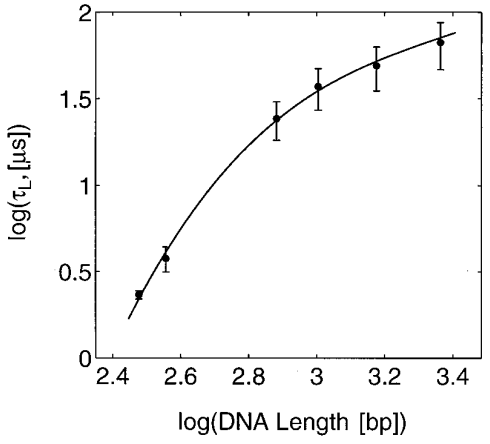

FIG. 10. Relaxation time of end-to-end distance versus DNA length. The BD simulation results are shown as filled circles along with the best quadratic fit. Results were obtained from the same trajectories used for Fig. 7.

end-to-end distance (l and L^2); translational diffusion constant, D_t; autocorrelation functions for L and selected angles θ; and rotational diffusion coefficient, D_r, with associated relaxation times. Both equilibrium and dynamic properties were compared to results of MC and experiment. Excellent agreement for our BD-generated results was demonstrated with respect to all available data.

In brief, we found the following.

1. Our choice for the virtual bond length ($l_0 = 5$ nm) satisfies two requirements: larger than the value corresponding to a touching-bead model, thereby making computational time manageable for long DNA, and sufficiently small to approximate well the electrostatic interaction and to prevent chain crossings.

2. Our calibrated bead radius (1.78 nm) yields the same frictional force as a touching-bead model and is close to the value obtained from the principle of equivalent chain volume [14].

3. The stretching potential of Eq. (2.1)—necessary for dynamic simulations—affects the realized bond variance (Fig. 2) as well as the timestep and simulation method used. A good compromise was found by setting the rigidity constant, h, to 100 $k_B T/l_0^2$.

4. Using the second-order BD method [18] gives roughly the same accuracy in comparison to the first-order scheme for more than double the timestep (Fig. 2). However, since each timestep of the second-order scheme is twice as expensive, our modification of the second-order method renders it more attractive (Table I). Namely, the elimination of auxiliary computations yields a CPU gain (with respect to the first-order method) that is essentially the timestep gain factor. Thus, we gain a factor of two speedup by using double the timestep.

5. Our BD results agree excellently with MC for the equilibrium property of end-to-end distance distributions (Fig. 4). MC is certainly very fast to propagate, but BD offers dynamic information.

6. Our BD results for the translational diffusion constant, D_t, agree very well with the experimental results, D^{Exp}, for the DNA systems tested in the range of 367 to 2311 bp (Table II and Fig. 6). In addition, good agreement between D_t and the MC result, D^{MC}, is obtained. Still, the small differences between D_t and D^{MC} that exceed statistical error might be due to the rigid-body approximation assumed in MC.

7. The decay of the logarithm of the second-order Legendre polynomial (see Eq. 5.2) can be well described by a single exponential for short chains (e.g., 300 bp), but multiexponential functions are needed to describe rotational motion of longer chains (e.g., 1500 bp) (Fig. 7). The rotational diffusion coefficients calculated for short chains (less than 750 bp) agree very well with the results of [16] obtained from a rigid-body approximation (Fig. 8).

8. Our illustrative dynamic result for the autocorrelation function of L (Fig. 9a) shows a good fit to a decaying exponential function of form $\exp(-t/\tau_L)$.

9. Our computed autocorrelation for the bond angle θ_i depends on chain position, i, but is independent of chain length (Fig. 9b).

The model has already been extended to treat closed circular DNA, where torsional motion and topological considerations are important [19]. Additions involve the torsional and torsional/bending terms, modified propagation scheme, and the treatment of the topological constraint of chain closure. These details, and interesting applications to branching and site juxtaposition, will be reported shortly [20].

APPENDIX A: BENDING RIGIDITY CONSTANT

The bending potential of our model chain is expressed in Eq. (2.2). Within this framework, when the number of links, N_b, is sufficiently large, the end-to-end distance squared can be written as

$$\langle L^2 \rangle = N_b \langle l \rangle^2 \left(\frac{1 + \langle \cos\theta \rangle}{1 - \langle \cos\theta \rangle} \right), \tag{A.1}$$

where

$$\langle \cos\theta \rangle = \frac{\int_0^\pi \cos\theta \sin\theta \exp(-g\theta^2/2k_B T)\, d\theta}{\int_0^\pi \sin\theta \exp(-g\theta^2/2k_B T)\, d\theta}. \tag{A.2}$$

Considering that the wormlike chain is a limiting case of our model chain, we can express N_b in terms of the number of Kuhn segments, m, by the relation [36]:

$$\frac{N_b}{m} = k = \frac{1 + \langle \cos\theta \rangle}{1 - \langle \cos\theta \rangle}. \tag{A.3}$$

Here k denotes the number of subsegments per Kuhn length. By solving Eq. (A.2) and (A.3), the dependence of g on k can be obtained. The obtained g is close to the result of pk_BT/l_0 used in [3, 5–7]. For example, when $k = 20$ and $p = 50$ nm, the values obtained by two approaches are 9.82 k_BT and 10 k_BT, respectively. However, as Frank-Kamenetskii *et al.* [12] showed, the above approach approximates a wormlike chain better in the range of small k (e.g., $k < 20$).

APPENDIX B: CHAIN HYDRODYNAMICS BY MONTE CARLO

As Zimm showed [39], certain dynamic properties of molecules in an applied external flow can be calculated as if their internal conformations are held fixed as far as the linear terms in the applied flow are concerned. To measure sedimentation, it is thus possible to calculate the average instantaneous force on any conformation of such molecules as if they were rigid. Zimm further demonstrated that it is sufficient to consider a component of the rotation around the sedimentation axis (z axis). Therefore, the motion of the molecule in a short period is considered as the combination of constant translation with velocity $\mathbf{u}$ and constant rotation around the z axis with angular velocity Ω_z. In the formalism of Kirkwood–Riseman, the frictional force exerted by ith bead on the fluid satisfies the series of equations

$$\mathbf{F}_i = \xi(\mathbf{u}_i - \mathbf{v}_{0i}) - \xi \sum_{j \neq i}^{N} \mathbf{T}_{ij} \cdot \mathbf{F}_j, \tag{B.1}$$

where $\xi = 6\pi\eta a$ and a is the radius of the bead. The vector $\mathbf{v}_{0i}$ denotes the externally-imposed flow that the fluid would have in the same experiment with the chain removed, and the matrix components $\mathbf{T}_{ij}$ are from the hydrodynamic interaction tensor, equal to $\mathbf{D}_{ij}/k_BT$ when $i \neq j$. At steady state at low flow rates, we have:

$$\begin{aligned} u_{ix} &= u_x - y_i\Omega_z \\ u_{iy} &= u_y + x_i\Omega_z \\ u_{iz} &= u_z. \end{aligned} \tag{B.2}$$

This gives a set of $3N$ equations with $3N + 4$ unknowns (the $3N$ component forces $\mathbf{F}$ together with u_x, u_y, u_z, and Ω_z) following the substitution of Eq. (B.2) into Eq. (B.1). Three additional relations can be added to the total sedimentation force, $\mathbf{F}$:

$$\sum_i \mathbf{F}_i = \mathbf{F}. \tag{B.3}$$

In our case, the x and y components of $\mathbf{F}$ are set to zero, while the z component was set to N, equivalent to a unit force in the z direction on each of the N beads. The fourth relation can be formulated from the fact that total torque around the z axis is zero, yielding:

$$\sum_i (y_iF_{ix} - x_iF_{iy}) = 0. \tag{B.4}$$

For any given conformation, we solve for the sedimentation velocity u_z from Eqs. (B1), (B.2), and (B.3). The translational diffusional frictional coefficient, f_0, can then be obtained as:

$$f_0 = F/\langle u_z \rangle. \tag{B.5}$$

By using Einstein's equation, we obtain the translation diffusion coefficient as:

$$D = \frac{k_BT}{f_0}. \tag{B.6}$$

ACKNOWLEDGMENTS

We are grateful to Gomathi Ramachandran for valuable discussions. We thank the Cornell Theory Center for granting computing resources on the Power Challenge system. Research was supported by the National Science Foundation and an Alfred P. Sloan research fellowship awarded to T. Schlick. T.S. is an investigator of the Howard Hughes Medical Institute.

REFERENCES

1. M. P. Allen and D. J. Tildesley, *Computer Simulation of Liquids* (Oxford Univ. Press, New York, 1994).
2. S. A. Allison, Brownian dynamics simulation of wormlike chains. Fluorescence depolarization and depolarized light scattering, *Macromolecules* **19,** 118 (1986).
3. S. A. Allison, R. Austin, and M. Hogan, Bending and twisting dynamics of short linear DNAs. Analysis of the triplet anisotropy of a 209 base pair fragment by Brownian simulation, *J. Chem. Phys.* **90,** 3843 (1989).
4. S. A. Allison and J. A. McCammon, Multistep Brownian dynamics: Application to short wormlike chains, *Biopolymers* **23,** 363 (1984).
5. S. A. Allison, S. S. Sorlie, and R. Pecora, Brownian dynamics simulations of wormlike chains: dynamic light scattering from a 2311 base pair DNA fragment, *Macromolecules* **23,** 1110 (1990).
6. G. Chirico and J. Langowski, Calculating hydrodynamic properties of DNA through a second-order Brownian dynamics algorithm, *Macromolecules* **25,** 769 (1992).

7. G. Chirico and J. Langowski, Kinetics of DNA supercoiling studied by Brownian dynamics simulation, *Biopolymers* **34,** 415 (1994).
8. G. Chirico and J. Langowski, Brownian dynamics simulations of supercoiled DNA with bent sequences, *Biophys. J.* **71,** 955 (1996).
9. P. de Gennes, *Scaling Concepts in Polymer Physics* (Cornell Univ. Press, Ithaca, NY, 1979).
10. D. L. Ermak and J. A. McCammon, Brownian dynamics with hydrodynamics interactions, *J. Chem. Phys.* **69,** 1352 (1978).
11. P. J. Flory, *Statistical Mechanics of Chain Molecules* (Wiley, New York, 1988).
12. M. D. Frank-Kamenetskii, A. V. Lukashin, and V. V. Anshelevich, Torsional and bending rigidity of the double helix from data on small DNA rings, *J. Biomol. Struct. Dynam.* **2,** 1005 (1985).
13. M. D. Frank-Kamenetskii and A. V. Vologodskii, Topological aspects of the physics of polymers: The theory and its biophysical applications *Sov. Phys. Usp.* **24,** 679 (1981).
14. J. Garcia de la Torre and V. A. Bloomfield, Hydrodynamic properties of macromolecular complexes. I. Translation, *Biopolymers* **16,** 1747 (1977).
15. P. J. Hagerman, Flexibility of DNA, *Ann. Rev. Biophys. Biophys. Chem.* **17,** 265 (1988).
16. P. J. Hagerman and B. H. Zimm, Monte Carlo approach to the analysis of the rotational diffusion of wormlike chains, *Biopolymers* **20,** 1481 (1981).
17. H. J. Heath, J. A. Gebe, S. A. Allison, and J. M. Schurr, Comparison of analytical theory with Brownian dynamics simulations for small linear and circular DNAs, *Macromolecules* **29,** 3583 (1996).
18. A. Iniesta and J. Garcia de la Torre, A second-order algorithm for the simulation of the Brownian dynamics of macromolecular models, *J. Chem. Phys.* **92,** 2015 (1990).
19. H. Jian, *A Combined Wormlike-Chain and Bead Model for Dynamic Simulations of Long DNA,* Ph.D. thesis (New York University, 1997).
20. H. Jian, V. A. Vologodskii, and T. Schlick, ''Internal motions of supercoiled DNA. Brownian dynamics simulations of site juxtaposition,'' manuscript in preparation, 1997.
21. K. V. Klenin, A. V. Vologodskii, V. V. Anshelevich, A. M. Dykhne, and M. D. Frank-Kamenetskii, Computer simulation of DNA supercoiling, *J. Mol. Biol.* **217,** 413 (1991).
22. R. T. Kovacic and K. E. van Holde, Sedimentation of homogeneous double-strand DNA molecules, *Biochemistry* **16,** 1490 (1977).
23. N. Metropolis, A. W. Rosenbluth, M. N. Rosenbluth, A. H. Teller, and E. Teller, Equation of state calculations by fast computing machines, *J. Chem. Phys.* **21,** 1087 (1953).
24. W. K. Olson, Simulating DNA at low resolution, *Curr. Opin. Struct. Biol.* **6,** 242 (1996).
25. R. Pecora, DNA: A model compound of solution studies of macromolecules, *Science* **251,** 893 (1991).
26. G. Ramachandran and T. Schlick, Solvent effects on supercoiled DNA dynamics explored by Langevin dynamics simulations, *Phys. Rev. E* **51,** 6188 (1995).
27. J. Rotne and S. Prager, Variational treatment of hydrodynamic interaction in polymers, *J. Chem. Phys.* **50,** 4831 (1969).
28. V. V. Rybenkov, N. R. Cozzarelli, and A. V. Vologodskii, Probability of DNA knotting and the effective diameter of the DNA double helix, *Proc. Natl. Acad. Sci. U.S.A.* **90,** 5307 (1993).
29. T. Schlick, Modeling superhelical DNA: Recent analytical and dynamic approaches, *Curr. Opin. Struct. Biol.* **5,** 245 (1995).
30. T. Schlick, B. Li, and W. K. Olson, The influence of salt on the structure and energetics of supercoiled DNA, *Biophys. J.* **67,** 2146 (1994).
31. T. Schlick and W. K. Olson, Supercoiled DNA energetics and dynamics by computer simulation, *J. Mol. Biol.* **223,** 1089 (1992).
32. T. Schlick and W. K. Olson, Trefoil knotting revealed by molecular dynamics simulations of supercoiled DNA, *Science* **257,** 1110 (1992).
33. S. Y. Shaw and J. C. Wang, Knotting of a DNA chain during ring closure, *Science* **260,** 533 (1993).
34. D. Stigter, Interactions of highly charged colloidal cylinders with applications to double-stranded, *Biopolymers* **16,** 1435 (1977).
35. R. K. Z. Tan and S. C. Harvey, Molecular mechanics model of supercoiled DNA, *J. Mol. Biol.* **205,** 573 (1989).
36. M. V. Volkenstein, *Configurational Statistics of Polymer Chains* (Wiley, New York, 1963).
37. A. V. Vologodskii and N. R. Cozzarelli, Conformational and thermodynamic properties of supercoiled DNA, *Ann. Rev. Biophys. Biomol. Struct.* **23,** 609 (1994).
38. A. V. Vologodskii and N. R. Cozzarelli, Modeling of Long-Range Electrostatic Interactions in DNA, *Biopolymers* **35,** 289 (1995).
39. B. H. Zimm, Chain molecule hydrodynamics by the Monte-Carlo method and the validity of the Kirkwood-Riseman approximation, *Macromolecules* **13,** 592 (1980).